This article was downloaded by: [b-on: Biblioteca do conhecimento online ITN]
On: 22 March 2012, At: 07:33
Publisher: Taylor & Francis
Informa Ltd Registered in England and Wales Registered Number: 1072954 Registered office: Mortimer House, 37-41 Mortimer Street, London W1T 3JH, UK

International Geology Review
Publication details, including instructions for authors and subscription information:
http://www.tandfonline.com/loi/tigr20

Mineralogy and geochemistry of tin- and germanium-bearing copper ore, Barrigão re-mobilized vein deposit, Iberian Pyrite Belt, Portugal

Fiona K.M. Reiser [a], Diogo R.N. Rosa [a b], Álvaro M.M. Pinto [b c], João R.S. Carvalho [b], João X. Matos [a], Fernanda M.G. Guimarães [a], Luís C. Alves [d] & Daniel P.S. de Oliveira [a b]

[a] LNEG/URMG, Alfragide, Portugal

[b] CREMINER/FCUL, Lisbon, Portugal

[c] Museu Nacional de História Natural da Universidade de Lisboa, Lisbon, Portugal

[d] ITN, Estrada Nacional, Sacavém, Portugal

Available online: 13 May 2010

To cite this article: Fiona K.M. Reiser, Diogo R.N. Rosa, Álvaro M.M. Pinto, João R.S. Carvalho, João X. Matos, Fernanda M.G. Guimarães, Luís C. Alves & Daniel P.S. de Oliveira (2011): Mineralogy and geochemistry of tin- and germanium-bearing copper ore, Barrigão re-mobilized vein deposit, Iberian Pyrite Belt, Portugal, International Geology Review, 53:10, 1212-1238

To link to this article: http://dx.doi.org/10.1080/00206811003683168

PLEASE SCROLL DOWN FOR ARTICLE

Full terms and conditions of use: http://www.tandfonline.com/page/terms-and-conditions

This article may be used for research, teaching, and private study purposes. Any substantial or systematic reproduction, redistribution, reselling, loan, sub-licensing, systematic supply, or distribution in any form to anyone is expressly forbidden.

The publisher does not give any warranty express or implied or make any representation that the contents will be complete or accurate or up to date. The accuracy of any instructions, formulae, and drug doses should be independently verified with primary sources. The publisher shall not be liable for any loss, actions, claims, proceedings,

demand, or costs or damages whatsoever or howsoever caused arising directly or indirectly in connection with or arising out of the use of this material.

Downloaded by [b-on: Biblioteca do conhecimento online ITN] at 07:33 22 March 2012

International Geology Review
Vol. 53, No. 10, 20 August 2011, 1212–1238

Downloaded by [b-on: Biblioteca do conhecimento online ITN] at 07:33 22 March 2012

Mineralogy and geochemistry of tin- and germanium-bearing copper ore, Barrigão re-mobilized vein deposit, Iberian Pyrite Belt, Portugal

Fiona K.M. Reiser[a]*, Diogo R.N. Rosa[a,b], Álvaro M.M. Pinto[b,c], João R.S. Carvalho[b], João X. Matos[a], Fernanda M.G. Guimarães[a], Luís C. Alves[d] and Daniel P.S. de Oliveira[a,b]

[a]*LNEG/URMG, Alfragide, Portugal;* [b]*CREMINER/FCUL, Lisbon, Portugal;* [c]*Museu Nacional de História Natural da Universidade de Lisboa, Lisbon, Portugal;* [d]*ITN, Estrada Nacional, Sacavém, Portugal*

(*Accepted 1 February 2010*)

The Barrigão re-mobilized copper vein deposit, Iberian Pyrite Belt, southern Portugal, is located about 60 km south of Beja and 10 km southeast of the Neves Corvo ore deposit, in Alentejo Province. The deposit is structurally associated with a NE–SW striking fault zone inferred to have developed during late Variscan deformation. The copper ore itself is a breccia-type ore, characterized by up to four ore-forming stages, with the late stages showing evidence of fluid-driven element re-mobilization. The ore is dominated by chalcopyrite+tennantite-tetrahedrite, with minor arsenopyrite, pyrite, and löllingite. The supergene paragenesis is composed mainly of bornite, covellite, and digenite. Whole-rock analyses show anomalous tin and germanium contents, with averages of 320 and 61 ppm, respectively. Electron microprobe analysis of Barrigão ores revealed the germanium and tin to be restricted to chalcopyrite, which underwent late-stage hydrothermal fluid overprint along distinct vein-like zones. The measured zonal enrichment of tin and germanium is related to limited element re-mobilization associated with mineral replacement, which resulted in distinctive mineral disequilibrium. Fluid-driven element zoning affected chalcopyrite and tennantite coevally. The average contents of germanium and tin in chalcopyrite are of 0.19 and 0.55 wt.%, respectively, as confirmed through additional micro-proton-induced X-ray emission (micro-PIXE) analysis. The distribution of tin and germanium in chalcopyrite correlates strongly with iron. Tin and germanium covary. Minute sub-microscopic inclusions of an unknown Cu–Sn–Ge sulphide phase have been detected in chalcopyrite and in small vugs therein. These inclusions hint at a stanniferous sulphide as the most possible host for tin and germanium in chalcopyrite, although the idea of limited incorporation of these two elements through element substitution cannot be completely excluded.

Keywords: germanium; high-technology elements; tin; Iberian Pyrite Belt; chalcopyrite; Barrigão ore deposit

Introduction

During the search for high-technology elements in a range of abandoned mines in the Portuguese sector of the Iberian Pyrite Belt (IPB), special interest in germanium (Ge) evolved from anomalously high tin (Sn) and Ge contents identified by means of whole-rock trace element analysis of copper ores from the abandoned Barrigão re-mobilized vein deposit.

*Corresponding author. Email: fiona.reiser@ineti.pt

ISSN 0020-6814 print/ISSN 1938-2839 online
© 2011 Taylor & Francis
DOI: 10.1080/00206811003683168
http://www.informaworld.com

Downloaded by [b-on: Biblioteca do conhecimento online ITN] at 07:33 22 March 2012

Gemanium is a trace element characterized by few accumulations of economic interest. The highly dispersed nature of Ge in the earth's crust complicates our understanding of the factors that control its deposition as discrete minerals or sequestered in other mineral phases, mainly sulphides and sulphosalts (such as sphalerite, enargite, germanite, and briartite), which make up the most important mineral class in terms of economic enrichment. A lack of study and knowledge on Ge-bearing sulphides still hampers their exploitation. Ongoing exploration for this element is of definite importance, considering that Ge is increasingly used in a range of high-tech applications, primarily in the growing thin-film, semiconductor, and fibre optics industries (Guberman 2009). Such demand results in a strong growth potential for the Ge market. As Ge does not form specific ore deposits but occurs in minor and trace amounts in a variety of ore types, its primary production is dependent on its profitability as a mining by-product. Currently, Ge is mainly recovered as a by-product of zinc production from sphalerite ores.

In contrast to Ge, Sn is typically concentrated in distinct deposits. Most of the world's Sn is produced from placer deposits, although porphyry-Sn-type lode deposits also play an important role. The only mineral of commercial importance is cassiterite (SnO_2). However, small quantities of Sn are recovered from complex sulphides, together with other metals like copper or lead. The number of technical applications for Sn is increasing, e.g. as a protective coating, as an alloy with other metals such as lead or zinc or as solder component, and for glass-making. As is the case for Ge, recycling is an important source of Sn supply, but to guarantee future element availability, the exploration for new deposits as well as the evaluation of known deposits for these elements is still a matter of considerable importance. Even though the Barrigão deposit, because of its limited dimension, will not play a role in terms of Ge extraction, the results from geochemical and mineralogical ore analysis contribute significantly to our knowledge of Ge distribution and deposition conditions within the IPB. The occurrence of Ge within the 'traditional' ores of the IPB could be of additional value for exploration criteria and adds new promise to existing mines for gaining extra revenue from the produced concentrates.

Geological setting

The Barrigão copper deposit is situated within the SE part of the Portuguese IPB, one of the richest mining districts in the world, hosting some of the largest concentrations of massive sulphides, including several giant or world-class volcanic-hosted massive sulphide (VHMS) deposits, e.g. Aljustrel and Neves Corvo, with the latter being located only 10 km northwest of the Barrigão mine (Figure 1). The IPB is considered to be one of five terranes which build the South Portuguese Zone and record the process of accretion to the Iberian massif during the subduction of the South Portuguese Plate beneath the Ossa Morena Plate (Quesada *et al.* 1991; Oliveira *et al.* 2006). The intercalated massive sulphide deposits are volcanogenic, strata-bound, and hosted in volcano–sedimentary successions of Late Devonian to Early Carboniferous age. The volcano–sedimentary successions underwent post-depositional low-grade regional metamorphism with thrusting and folding during the Variscan orogeny in Early to Late Carboniferous times (Leistel *et al.* 1998). Variscan deformation resulted in the tectonic dismembering of the volcano–sedimentary successions and ore deposits as well as in the development of late fault-related veins, distributed throughout the South Portuguese and Ossa Morena zones, often hosting copper deposits similar to Barrigão (Mateus *et al*. 2003; Matos *et al.* 2003). Exploitation of these veins took place mainly in the second part of the nineteenth century, sometimes down up to a depth of 100 m. Their supergene enrichment zones, represented by copper (Cu) and iron

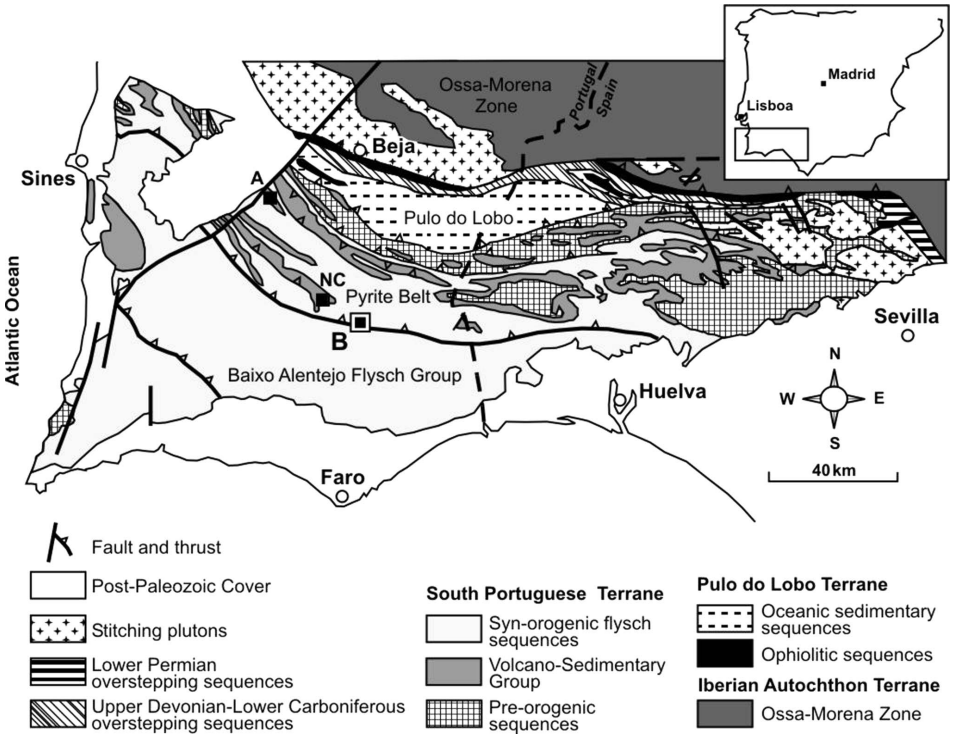

Figure 1. Geological setting of the Iberian Pyrite Belt (IPB) and the location of the Barrigão vein deposit within the IPB. A – Aljustrel; NC – Neves Corvo; B – Barrigão (adapted after Rosa *et al.* 2009).

(Fe) minerals, e.g. malachite, hematite, azurite, and tenorite, have been mined during Roman and possibly even earlier, in Chalcolithic, times.

The Barrigão deposit (Figure 2) consists of two converging metric thick vein structures, extending approximately 1800 m along strike (Matos and Rosa 2001; Matos *et al.* 2003). Several small secondary vein structures branch off the main structures. The veins cross-cut Visean shales and greywackes of the Mértola Formation, a subunit of the Baixo Alentejo Flysch Group (Oliveira *et al.* 2006). Exploration drilling carried out by SOMINCOR (Sociedade Mineira de Neves Corvo, SA) 2.5 km northeast of the old mine workings confirmed that the Mértola Formation continues at least down to a depth of 1140 m (Matos and Rosa 2001). Copper ore extraction was carried out in the second half of the nineteenth century. From 1965 to 1973, the state-owned Serviço de Formento Mineiro (SFM) executed extensive pilot exploitation for copper reserves in the pre-existing mine galleries (Ferreira *et al.* 1995), which resulted in several dumps from which the study samples have been collected.

The age of the Barrigão vein deposit and other similar copper structures in the region (Brancanes, Ferrarias/Cova dos Mouros etc.) is considered to be late Variscan with possibly an Eo-Alpine overprint. In the Ossa Morena Zone copper veins, chalcopyrite deposition mainly took place at temperature conditions of 260–300ºC under $10^{-33} < fO2 < 10^{-28}$ for a wide range of fluid salinities ($2 \leq$ wt.% NaCl ≤ 25) and as a result of local temperature decrease, H_2S concentration increase, salinity depletion, reduction, and/or pH rise (Mateus

Downloaded by [b-on: Biblioteca do conhecimento online ITN] at 07:33 22 March 2012

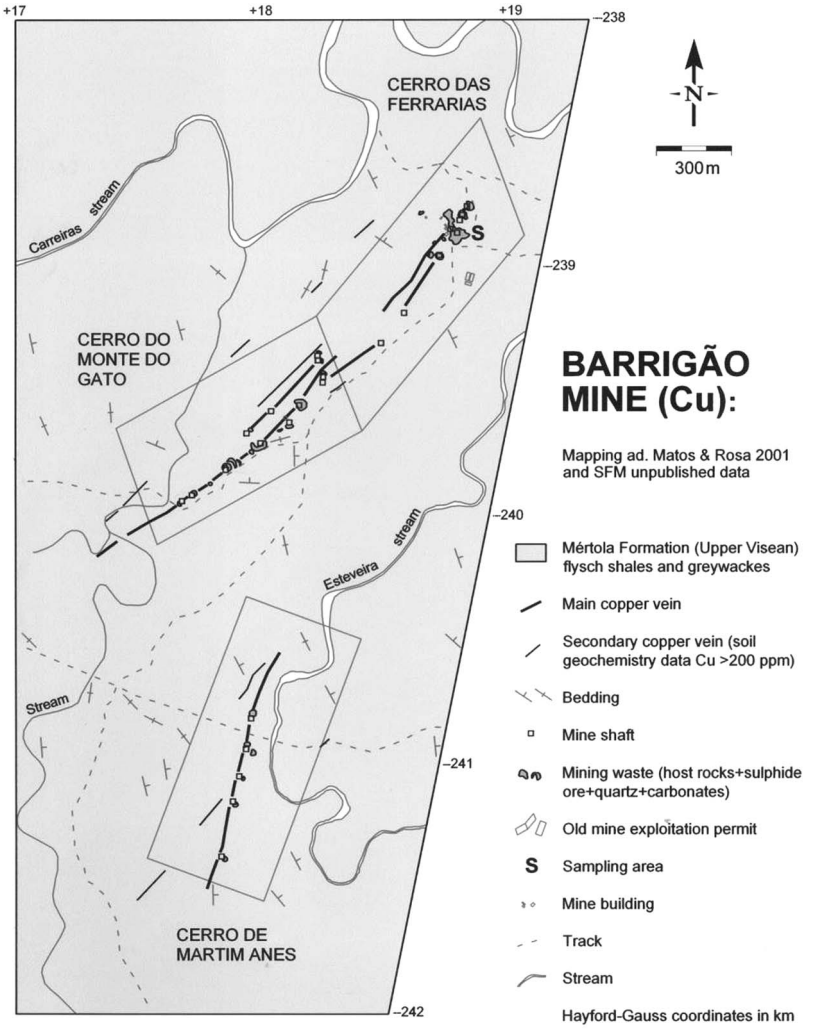

Figure 2. Structural map of the Barrigão re-mobilized vein deposit. The anastomosing vein system, consisting of two major and several minor veins, cross-cuts a thick sequence of shales and greywackes of the Mértola Formation.

et al. 2003; Matos *et al.* 2003). These structures are intimately related with the main fault systems present in the southeastern sector of the South Portuguese Zone, striking generally NE–SW and NW–SE and controlling the regional drainage pattern. The distribution of these copper structures and their location southeast of Neves Corvo were formerly considered an indication for massive sulphide exploration (Carvalho 1982). However, their sparse occurrence in the South Portuguese and Ossa Morena zones does not correlate directly with the presence of massive sulphide bodies.

Germanium and tin mineralogy

Germanium was first detected in 1886 by the German chemist, Clemens Winkler, as a constituent of the silver sulphide mineral agyrodite (Ag_8GeS_6). Germanium is a geological

Downloaded by [b-on: Biblioteca do conhecimento online ITN] at 07:33 22 March 2012

all-round element, as it can behave distinctly, as lithophile, siderophile, chalcophile, and organophile, in different geological environments. It is geochemically scarce, with an estimated crustal average of about 1.6 ppm (Taylor and McLennan 1985). Most of the Ge contained in the earth's crust is finely dispersed through silicate phases, but high and economically interesting concentrations are found in zinc- and copper-rich sulphide ore deposits or in coal and lignite. Grades of a few tens to several hundred ppm of Ge are known from sulphide ore deposits (Höll *et al.* 2007), including VHMSs, porphyry and vein-stockwork deposits, sediment-hosted massive sulphides, carbonate-hosted Zn–Pb deposits, and polymetallic Kipushi-type deposits. Economic Ge contents (with values up to a few hundred ppm) are also found in specific coal deposits (Gang *et al.* 2009).

Germanium generally occurs in the tetravalent state, therefore developing tetrahedral coordination. Its high electronegativity favours covalent bonds and the similar ionic radius to silicon leads to isomorphous substitution for silicon in a range of silicates (Bernstein 1985). Germanium can also occur in sixfold coordination in some oxide and hydroxide minerals substituting for Fe, e.g. in goethite and stottite (Höll *et al.* 2007). Regarding the occurrence of high Ge contents in the Barrigão chalcopyrite, it is important to note that Ge can be an essential component of a range of sulphide minerals such as germanite, renierite, briartite, or argyrodite, in which it usually favours tetrahedral coordination. In Ge-bearing sulphide ore deposits, Ge can be present as discrete mineral phases or such phases occur as micro-inclusions in other sulphides. Tin-bearing sulphides, e.g. the stannite-kesterite solid-solution series, structurally similar to briartite, are known to be able to substitute Ge for tetravalent Sn in the crystal lattice (Bernstein 1985). The economically most important sphalerite contains Ge either as sub-microscopic inclusions of thiogermanates (renierite, briartite) or as elemental Ge substituting for zinc (Johan 1988; Cassard *et al.* 1996). High Ge concentrations are found in enargite (5000 ppm), sphalerite (3000 ppm), stannite (2830 ppm), tennantite (1500 ppm), and colusite and sulvanite (up to 1000 ppm; data from Höll *et al.* 2007). Most of these minerals have sphalerite or sphalerite derivate structures.

Tin was known as early as the Bronze Age. The first large-scale use of Sn was as an alloy together with copper in bronze. In contrast to Ge, Sn is slightly more abundant in the earth's crust (2 ppm). Elemental Sn is tetragonal but Sn can occur as a divalent as well as tetravalent cation. It shows similar chemical behaviour to its two neighbouring elements in the periodic table, Ge and lead, e.g. with the two possible oxidation states, +II and+IV. The most abundant Sn mineral, which is at the same time the most economically important, is cassiterite, often associated with tungsten minerals in high-temperature veins related to igneous rocks. Tin is also a major component of the stannite group minerals and of some sulphosalts (e.g. teallite). Stannite group minerals and Sn-bearing sulphosalts mainly occur in hydrothermal vein ores but are also reported from VHMS deposits, e.g. from the Neves Corvo mine (Benzaazoua *et al.* 2003). Furthermore, Sn has been reported to be contained as a trace component in usually Sn-free sulphides, such as sphalerite and chalcopyrite, where it is considered to enter the crystal structure through coupled substitution with zinc and iron (Gena 2005; Cook *et al.* 2009). Elemental Sn is found in small irregular rounded grains in placer deposits, unspecified kimberlite pipes, and seafloor spreading zones. In its elemental occurrence, it is often associated to platinum group elements (PGEs), gold, Cu, and cassiterite.

Sampling and analytical methods

Due to the impossibility of safe underground mine access, ore samples of ~0.5–6 kg were collected from the mine dumps located in the northern sector of the Barrigão mine (Figure 2).

Downloaded by [b-on: Biblioteca do conhecimento online ITN] at 07:33 22 March 2012

For whole-rock analysis preparation, 10 samples with varying ore contents were selected and subsequently cut and milled, avoiding contamination through equipment, weathered cracks, and crust. Milling was performed using agate rings. The analysis process for trace elements has been carried out using a combination of instrumental neutron activation analysis (INAA) and inductively coupled plasma–mass spectrometry (ICP-MS) at Activation Laboratories Ltd., Ancaster, Ontario, Canada. The 10 whole-rock samples, together with an additional 12 ore and host-rock samples, were prepared as polished blocks and thin sections for optical microscopy and micro-analysis.

A total of 10 polished ore sections were selected for micro-analysis and element mapping by electron probe micro-analysis (EPMA), which was performed at the LNEG Laboratory in São Mamede de Infesta, Portugal. Analysis was carried out using a fully automated JEOL JXA-8500F microprobe operating in wavelength dispersive spectroscopy (WDS) mode at 20 kV excitation voltage and 20 nA beam current to produce an electron beam of 1 μm diameter for analysis of S, Fe, Cu, As, Sb, Zn, Pb, Sn, Ge, Cd, Se, Bi, Ni, Co, Mn, Ag, Hg, V, and In. The following standards, analytical lines, and crystals were used: S (FeS_2) Kα-PET, Fe (FeS_2) Kα-LIF, Cu (Cu_2O) Kα-LIF, As (AsGa) Lα-TAPH, Sb (Sb_2S_3) Lα-PETH, Zn (ZnS) Kα-LIF, Pb (PbS) Mα-PET, Sn (SnO_2) Lα-PETH, Ge (Ge) Lα-TAPH, Cd (CdS) Lα-PET, Se (Bi_2Se_3) Lα-TAPH, Bi (Bi_2Se_3) Mα-PET, Ni (Ni) Kα-LIF, Co (Co) Kα-LIF, Mn ($MnTiO_3$) Kα-LIF, Ag (Ag) Lα-PET, Hg (HgS) Mα-LIFH, V ($Pb_5(VO_4)_3Cl$) Kα-LIFH, In (InP) Lα-PETH.

Additionally, for micro-proton-induced X-ray emission (Micro-PIXE) analysis of trace element contents and distributions in chalcopyrite, eight polished blocks and three polished thin sections were used. Initially, Ge detection was tested with a polished section of germanite, from Tsumeb, Namibia. Analysis has been carried out at the Instituto Tecnológico e Nuclear (ITN) in Sacavém, Portugal, using an Oxford Microbeams nuclear microprobe able to focus down to 3×4 μm^2 with a 2 MeV proton beam generated by a 2.5 MV Van den Graaff accelerator. The focused proton beam was raster-scanned over the samples and the produced X-rays were collected with an 80 mm^2 and 145 eV resolution Si (Li) detector positioned at 45° to the beam direction, protected by a 50 μm Mylar filter. A 200 mm^2 Si particle detector positioned at 40° to the beam direction was used to detect backscattered particles (Rutherford backscattering spectrometry, RBS) and was mainly employed for beam charge normalization. Microprobe control and data handling were accomplished through OMDAQ (Grime and Dawson 1995) computer code, which also allowed obtaining elemental distribution maps. The proton beam current was kept between 100 and 200 pA. A large beam scan (max. of 2640×2640 μm^2) was applied in zones previously selected by optical microscopy with subsequent zooming according to the details required by the observed sample structure, down to an area of 264×264 μm^2. Selective point analysis was performed in order to obtain quantitative results, using the GUPIX code (Maxwell *et al.* 1995) included in the DAN32 (Grime 1996) software package.

Petrography and ore paragenesis

Ore assemblage

The Barrigão copper ore is represented by fault breccias composed of chalcopyrite, tennantite, tetrahedrite, and pyrite, with minor or rare arsenopyrite, löllingite, sphalerite, native bismuth, and an undetermined Cu–Sn–Ge-sulphide in a matrix of quartz, angular fragments of black shale, and carbonate minerals (Figure 3). The host rocks are siliceous greywackes and shales, consisting of quartz, feldspar, muscovite, plagioclase, chlorite,

Downloaded by [b-on: Biblioteca do conhecimento online ITN] at 07:33 22 March 2012

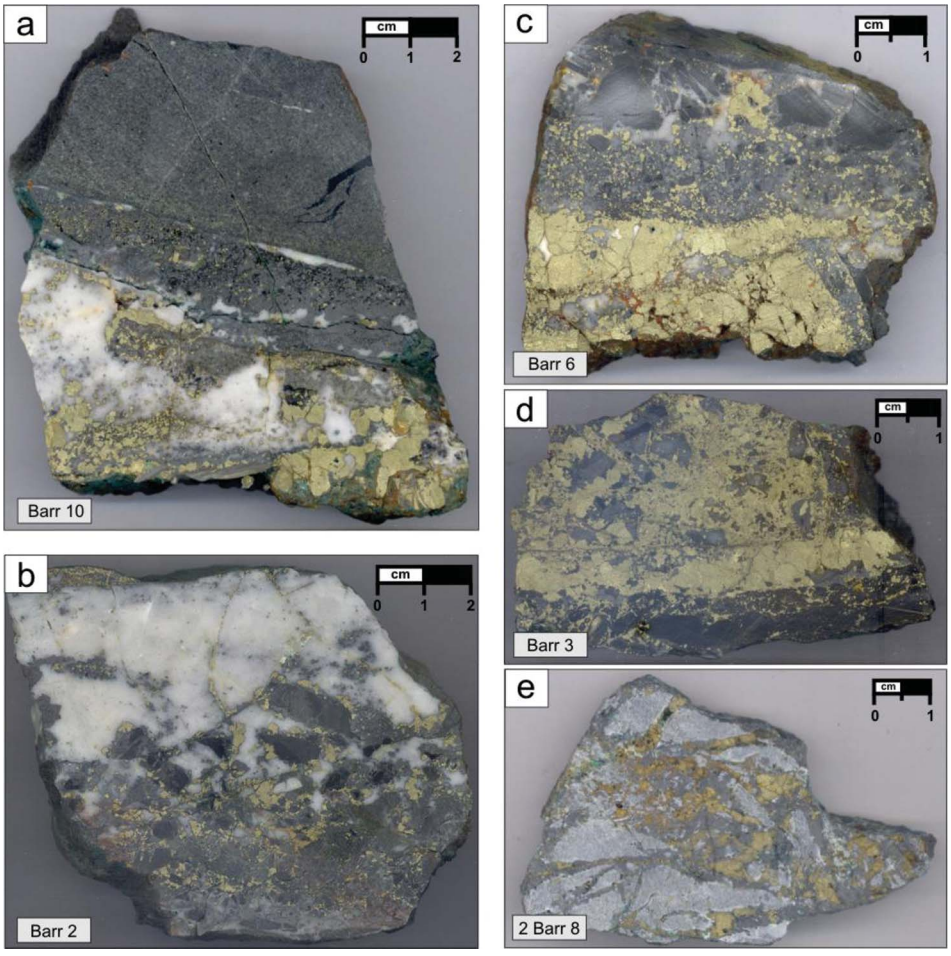

Figure 3. Typical Barrigão ore samples. (a) Silicified host rock cross-cut by zoned ore vein consisting of a marginal zone of tn-td with fine-grained disseminated cp and some quartz and gangue, grading into a quartz-rich zone with disseminated and coarse cp aggregates (Barr 10). (b) Quartz-rich vein sample with dark shale clasts, which are concentrically rimmed by tn-td and cp (Barr 2). (c) Typical breccia ore showing indistinct layering of (from bottom to top) coarse-grained cp and a medium- to fine-grained tn-cp paragenesis, with small shale fragments grading into a zone of dark shale with interstitial quartz and carbonate (Barr 6). (d) Zoned ore sample with dark shale containing disseminated cp adjoining a coarse-grained layer-like cp zone with minor tn. Replacement cp (ore stage III) with abundant inclusions of fine-grained quartz and some relict tn-td. This paragenesis contains Sn–Ge-rich cp (Barr 3). (e) Silicified host rock showing an irregular vein network of a cp-tn assemblage (ore stage III) with a porous aspect and supergene overprint. Veins are bordered by small carbonaceous rims. The weathering product in vugs is malachite. The cp contains Sn–Ge-rich zones (2 Barr 8).

rutile, apatite, and graphite, with the latter sometimes locally enriched. Schistosity of the host rocks developed through strong foliation of mica and, where present, graphite.

The host rocks are often cross-cut by millimetre-wide quartz and calcite veins. Dark shale clasts and siliceous host rocks adjacent to the ore veins often exhibit traces of disseminated pyrite, in places framboidal, and chalcopyrite. Feldspar is partly altered to sericite and occasionally shows initial re-crystallization. Rarely, calcite is present near

Downloaded by [b-on: Biblioteca do conhecimento online ITN] at 07:33 22 March 2012

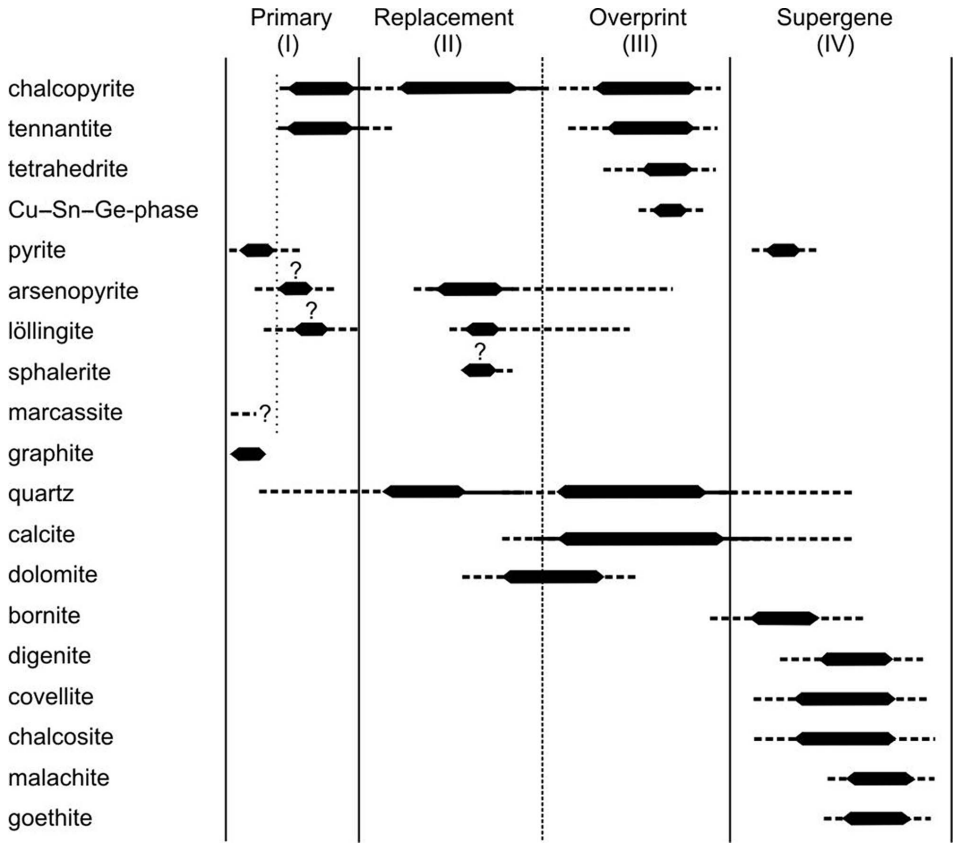

Figure 4. Inferred paragenetic sequence and ore stages of the Barrigão ore.

calcite-bearing late veins. Calcite seldom shows re-crystallization phenomena, whereas quartz grains in the host rocks and small cross-cutting quartz veins can be completely re-crystallized. These quartz veins cross-cut the schistosity of the host rock at high angles. Zoned carbonate-bearing veins, which often contain chalcopyrite and/or tennantite in the centre, associated with euhedral quartz, cross-cut early quartz veins. Due to late tectonics overprint, all quartz generations occurring within Barrigão mineralization do not contain adequate fluid inclusions to perform relevant studies.

Ore formation took place in several phases, some of which are well preserved in the ore textures. Macroscopic and microscopic investigation permits the distinction of at least four texture types, allowing a provisional classification into four ore stages (Figure 4):

Primary assemblage

The naming ‘primary’ for this ore paragenesis refers to the early stage of ore formation (ore stage I), which is characterized by the lack of Sn and Ge in the related chalcopyrite (cp). When looking at hand specimens, medium-grained layer-like zones and aggregate areas of predominantly chalcopyrite or tennantite (tn) occur in individual spatial distribution (Figures 3a, c). However, coexistence of subhedral to euhedral chalcopyrite with tennantite in grain sizes up to 1 cm is common (Figure 3b). This early chalcopyrite (cp I)

Downloaded by [b-on: Biblioteca do conhecimento online ITN] at 07:33 22 March 2012

predominantly formed in equilibrium with tennantite (Figure 5e). Under the microscope, the chalcopyrite and tennantite grains can appear nearly inclusion-free. Occasionally, chalcopyrite hosts small subhedral pyrite relics (up to 10 μm), which themselves can contain marcasite relics and/or euhedral löllingite.

Replacement assemblage

More often, chalcopyrite and tennantite occur intimately intergrown on macroscopic (Figure 3d) and microscopic (Figure 5a) scale, with subhedral chalcopyrite hosting abundant subhedral to anhedral tennantite relics, sometimes in atoll-like morphologies, and less euhedral arsenopyrite (1–5 μm across). Tennantite itself can contain minute to small (1–20 μm) subhedral chalcopyrite "inclusions", sometimes aligned along crystal faces, which are interpreted as atoll-like structures due to incomplete replacement of tennantite by chalcopyrite. These textures are often accompanied by minute arsenic-rich phases (mostly arsenopyrite) in contact with both chalcopyrite and tennantite, and are characteristic of ore stage II. Further evidence for a replacement process of tennantite (tn I) through secondary chalcopyrite (cp II) is fractured tennantite grains included in otherwise nearly inclusion- and fracture-free chalcopyrite (Figure 5b). In one single sample, chalcopyrite (Barr 3-3) contains minute marginal inclusions inferred to be sphalerite (< 2 μm) by means of microscopic investigation, possibly a minor product of tennantite decomposition. In places, chalcopyrite has been observed to contain orientated marginal inclusions of graphite, indicating its overgrowth over former schist clasts. Tennatite, where it is not extensively replaced, shows concentric compositional growth zoning, in places almost perfectly developed (Figure 5f). The occasional occurrence of native bismuth grains is restricted to tennantite. Both chalcopyrite and tennantite can host euhedral inclusions of quartz.

On both the macroscopic and microscopic scale, concentric mineral zoning is observable on dark graphite-bearing shale clasts, which form a frequent constituent of the ore gangue. These clasts are often rimmed by a thin layer of quartz, followed by tennantite, which itself is rimmed by chalcopyrite (Figure 3b).

Hydrothermal overprint assemblage

Textures associated with hydrothermal overprint (ore stage III) include quartz-carbonate veins showing dynamic re-crystallization and fragment transport of anhedral chalcopyrite, tennantite, and schist, with the fragments often being marginally corroded or spotted with euhedral quartz inclusions. Tennantite and chalcopyrite grains of the former main ore stage (II) are often fractured to varying degrees. Intensified brecciation fabric together with quartz and calcite veins may hint at high fluid pressure during ore breccia formation. Tectonic contacts, e.g. of more rigid, chalcopyrite-rich layers against quartz-calcite veins, and discrete brittle 'micro fault-planes' are sometimes visible in hand specimens and under the microscope. Hydrothermal fluid overprint led to partial decomposition of tennantite and chalcopyrite, indicated by corroded margins and re-deposition of chalcopyrite (cp III), nearly pure end-member tennantite, and a fahlore closer to the tetrahedrite end-member composition of the tetrahedrite-tennantite solid-solution series in small micro-veins or disseminated in host-rock breccia. This ore paragenesis is characterized by abundant euhedral quartz present as individual grains or small grain aggregates in tennantite and chalcopyrite (Figure 5g). The fluid overprint was clearly of a polyphase character. In places, quartz veins are cross-cut or 'reopened' by later quartz-carbonate veins, with the latter also being chalcopyrite-bearing.

Downloaded by [b-on: Biblioteca do conhecimento online ITN] at 07:33 22 March 2012

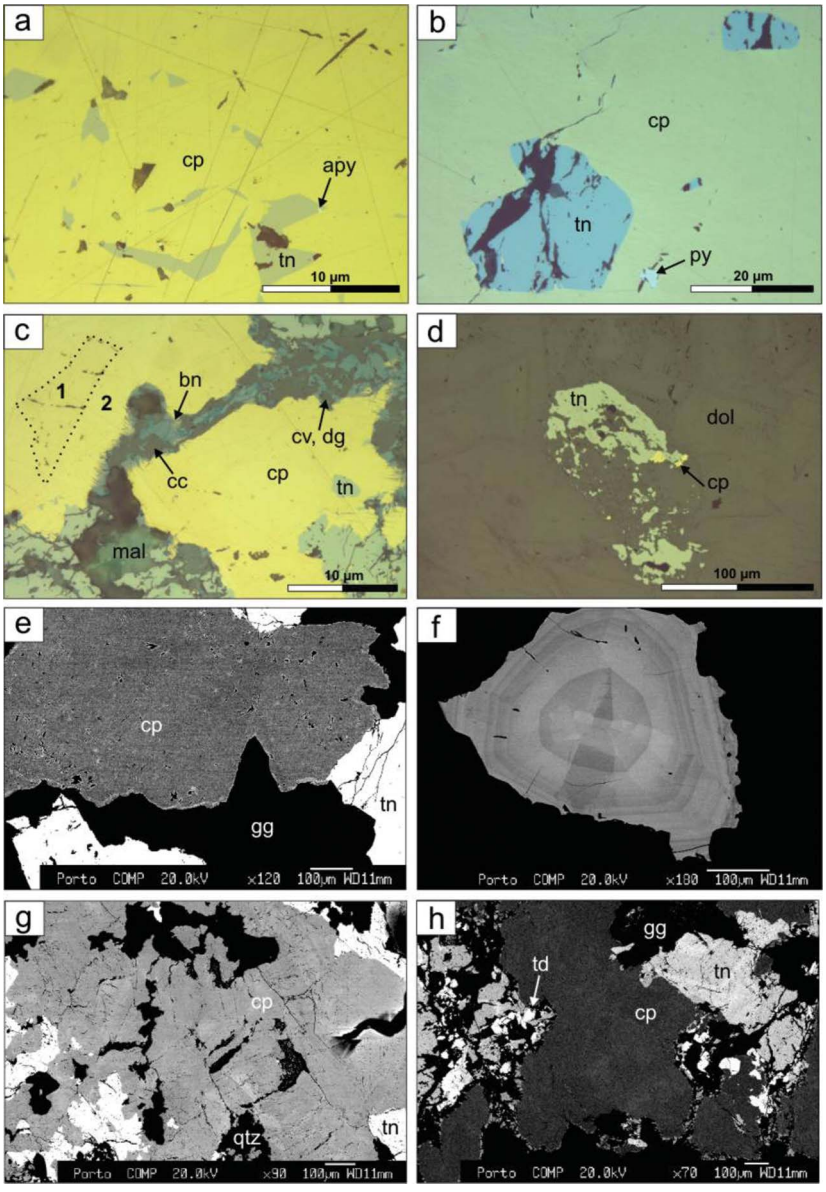

Figure 5. Ore microscope and EBS images of typical Barrigão ore assemblages and textures. (a) Replacement texture (ore stage II) with atoll-like tn relics and small euhedral apy in cp (Barr 6). (b) Fractured tn relics and small py in nearly fracture- and inclusion-free stage (II) replacement cp (Barr 3-2). (c) Zoned cp (slightly visible) with older cp relict (1) in younger cp (2). The younger cp is of stage (III) hydrothermal overprint assemblage. Surrounding tn is fractured, inclusion-rich, and altered. The overprinting supergene stage (IV) assemblage consists of bn, cv, dg, and cc. Late Fe oxides and malachite fill vugs. The young cp contains Sn and Ge (2 Barr 8). (d) 'Dissolved' tn and some cp replaced by late dol (2 Barr 16). (e) Primary (ore stage I) assemblage of cp and tn in gangue (Barr 6). (f) Stage (I) tn with a well-developed concentric and sector zoning in gangue. Bright zones are richer in antimony. Note the 'corroded' margin on the right which developed disequilibrium overprint (Barr 3). (g) Hydrothermal overprint assemblage (ore stage III) with slightly zoned cp hosting tn relics and quartz inclusions (Barr 1). (h) Supergene overprint on stage (III) assemblage with slightly zoned cp, tn, and late td and supergene copper sulphides (bn, cv, dg, cc) (2 Barr 8).

Downloaded by [b-on: Biblioteca do conhecimento online ITN] at 07:33 22 March 2012

Supergene assemblage

The supergene mineral assemblage (ore stage IV) consists predominantly of covellite, digenite, and chalcocite, replacing chalcopyrite marginally and through cross-cutting veins which fill former fractures (Figures 5c, h). Bornite occurs as a minor constituent in this paragenesis, initially replacing chalcopyrite and itself being replaced by covellite and chalcocite. Digenite and chalcocite replace tennantite along cracks and fractures. The supergene copper enrichment was triggered by copper-enriched fluids descending from the oxidation zone. Malachite, subordinate azurite, and limonite and other Fe hydroxides make up the oxidized mineral fraction, hosted in vugs and along cracks (Figure 3e). Relics of magnetite, which have been converted to goethite, can be found in the gangue. Anastomosing carbonaceous micro-veins occur in tennantite and chalcopyrite. Late-stage pyrite occurs in vugs and open space fillings or as fine-grained agglomerations in chalcopyrite.

Downloaded by [b-on: Biblioteca do conhecimento online ITN] at 07:33 22 March 2012

Host-rock veins

Host-rock veins are of different sizes and compositions, indicating an episodic passage of hydrothermal fluids of different compositions, which reflect the polyphase and presumably fault-related evolution of the ore deposit. First, a network of small quartz veins can be observed, with dimensions of a few millimetres' width, possibly indicating initial fault-related hydro-fracturing, overprinted by at least two more vein stages. The initial veins are completely re-crystallized and cross-cut by younger quartz or quartz-calcite veins. Veins which host more than one phase are generally symmetrically zoned. The paragenesis of these veins is quartz + calcite/dolomite (+chalcopyrite/tennantite), with the ore phases being mostly subhedral where unaffected but sometimes able to appear as partly replaced through calcite or dolomite (Figure 5d). The vein texture is either blocky or of stretched type and veins are mostly from ~1 mm up to 1 cm wide. Textural evidence suggests that the vein carbonates precipitated during the late stage of hydrothermal activity (ore stage III), following the main stage of ore formation (ore stage II), which has been accompanied by abundant quartz. Pure calcite veins and carbonate micro-veins within the sulphide phases are late. These calcite veins (1 mm to >1 cm wide) are of blocky appearance and cross-cut older quartz and quartz-calcite/dolomite-ore-bearing veins. Adjacent to calcite veins, the host-rock shales and greywackes often show a zone of calcite enrichment. Thin discontinuous calcite veins at high angle to and cross-cutting polyphase veins also occur, possibly indicating limited late-stage calcite re-mobilization.

Whole-rock geochemistry

Whole-rock analysis has been carried out on 10 ore samples collected from the mining dumps. The ore samples revealed anomalous Sn and Ge contents with an average of 320 and 61 ppm, respectively, ranging between 16 and 872 ppm for Sn and 4 and 280 ppm for Ge (Table 1). The outstanding values of Sn and Ge indicate their heterogeneous distribution in the ores, coevally implying their connection to distinct mineral phases. The wide range of values of whole-rock analysis data results from the variety of samples collected: some Barrigão samples actually contain more gangue material than sulphide minerals, therefore exhibiting lower Cu, As, Ge, etc., contents.

Compared to IPB massive sulphide deposits (MS in Figure 6a), e.g. Feitais/Aljustrel and Lagoa Salgada (Gaspar 1996; De Oliveira *et al.* submitted), the Barrigão ore clearly shows a distinct signature, due to its different nature of formation. It is distinguished by

Downloaded by [b-on: Biblioteca do conhecimento online ITN] at 07:33 22 March 2012

Table 1. Whole-rock analysis of Barrigão ore samples.

Sample	Cu %	S %	Fe %	Al %	As %	Sb %	Ca %	Mg %	P %	Zn ppm	Bi ppm	Sn ppm	Ge ppm	Pb ppm	Ag ppm	In ppm
Barr 1	24,20	18,20	13,90	1,26	2,07	1,17	0,56	0,21	0,16	844	173	710	84,8	120	65	2
Barr 2	13,80	8,65	4,55	2,09	2,49	1,76	0,88	0,36	0,08	2050	349	106	15,5	13	188	5
Barr 3	27,50	>20.0	16,40	0,95	3,11	1,23	0,36	0,09	0,15	1090	245	872	280	30	76	2
Barr 4	15,60	12,30	11,00	2,17	2,13	0,22	0,44	0,25	0,14	333	343	338	19,6	7	30	2
Barr 5	4,18	3,03	1,69	7,28	1,36	0,58	0,11	0,05	0,05	460	135	16	9,3	16	39	1
Barr 6	21,60	17,50	14,10	2,13	1,67	1,07	0,17	0,19	0,11	1250	264	399	90,4	16	48	5
Barr 7	23,00	14,90	6,55	1,23	5,95	1,43	0,24	0,06	0,11	5500	1070	149	11,4	31	142	7
Barr 8	18,80	13,30	10,40	1,54	1,86	1,02	0,98	0,41	0,13	1000	175	308	54,9	16	48	2
Barr 9	11,20	8,67	9,88	1,37	0,06	0,05	2,92	1,4	0,22	76	44,9	252	41,5	7	5	2
Barr 10	16,40	9,05	4,48	3,08	4,33	1,46	2,18	1,33	0,10	920	720	43	3,9	3	134	4

Whole-rock analysis has been performed through Activation Laboratories Ltd., Ancaster, Ontario, Canada
Analysis methods were as follows:
TD-MS for Bi, Ge, ln
TD-ICP for S, Al, Ca, Mg, P, Zn, Pb, Ag,
INAA for Fe, As, Sb
FUS-MS-Na2O2 for Cu, Sn.

high Cu (17.6% average) and As (25,000 ppm average) as well as by relative enrichment in Bi and Ag. On the other hand, the Barrigão deposit is relatively depleted in Fe, Zn, Pb, and In (Table 1 and Figure 6a). Compared to semi-massive and massive Cu-rich ores (MC and MS ores after Relvas *et al.* 2006) from the Neves Corvo deposit (NC in Figure 6a), the Barrigão ore shows similar Cu values but contains less Sn. However, when compared to Neves Corvo Cu ores, the Barrigão ore is significantly enriched in As.

Regarding only the Barrigão data, whole-rock analysis shows a positive correlation between Cu–S, Cu–Fe, Cu–Ge, and Cu–Sn, indicating that Ge and Sn are likely to be incorporated into some copper sulphide phase. Furthermore, Sn and Ge are obviously associated to high whole-rock Fe contents (Table 2). There is also positive correlation between Ge and Sn, showing the close association of these two elements. Positive correlation of In with Cd, Zn, Bi, As, and Ag leads to the assumption that the In contents, although

Downloaded by [b-on: Biblioteca do conhecimento online ITN] at 07:33 22 March 2012

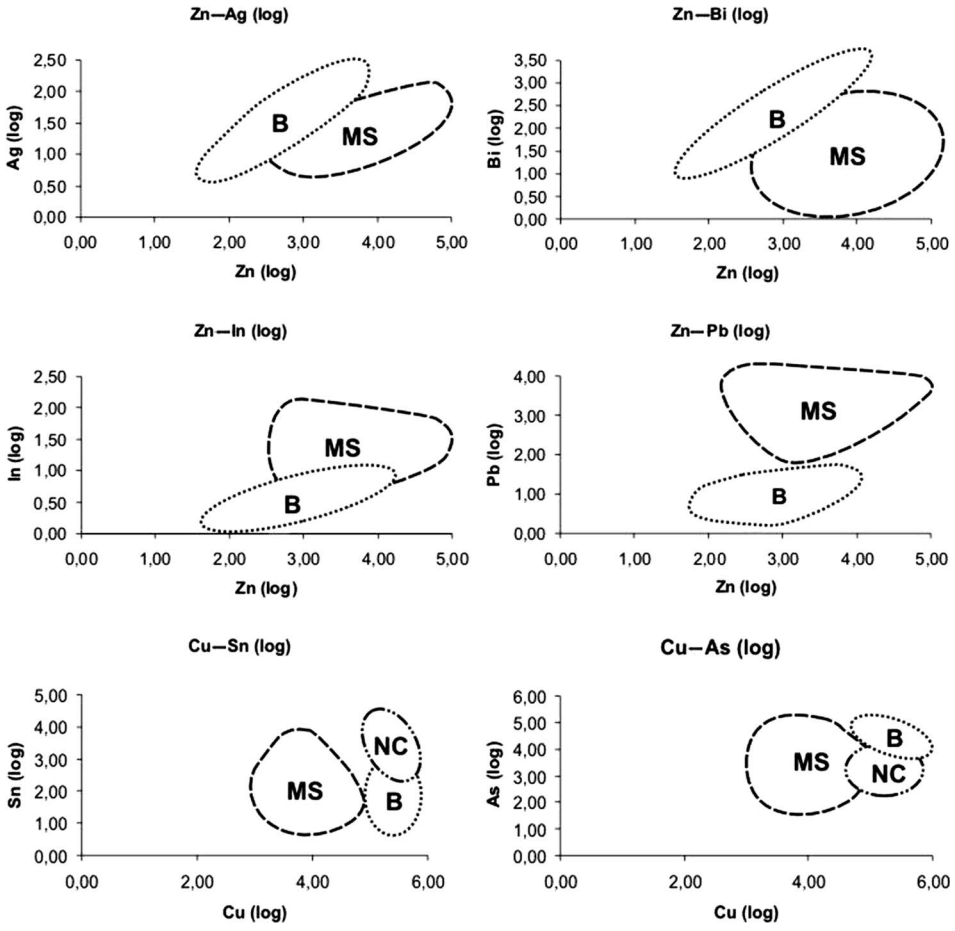

Figure 6. (a) Barrigão (B), IPB massive sulphide (MS), and Neves Corvo (NC) deposit whole-rock analysis element correlations showing the distinct character of the Barrigão ores. MS data include whole-rock analyses of the Lagoa Salgada (De Oliveira *et al.* submitted) and Feitais (Gaspar 1996) deposits. Neves Corvo Cu-rich (MC ore) and Cu–Sn-rich (MS ore) data extracted from Relvas *et al.* (2006). (b) Trace element correlations in typical Sn–Ge-rich chalcopyrite of the samples Barr 1 and 2 Barr 8. Black diamonds – Barr 1; grey squares – 2 Barr 8.

Downloaded by [b-on: Biblioteca do conhecimento online ITN] at 07:33 22 March 2012

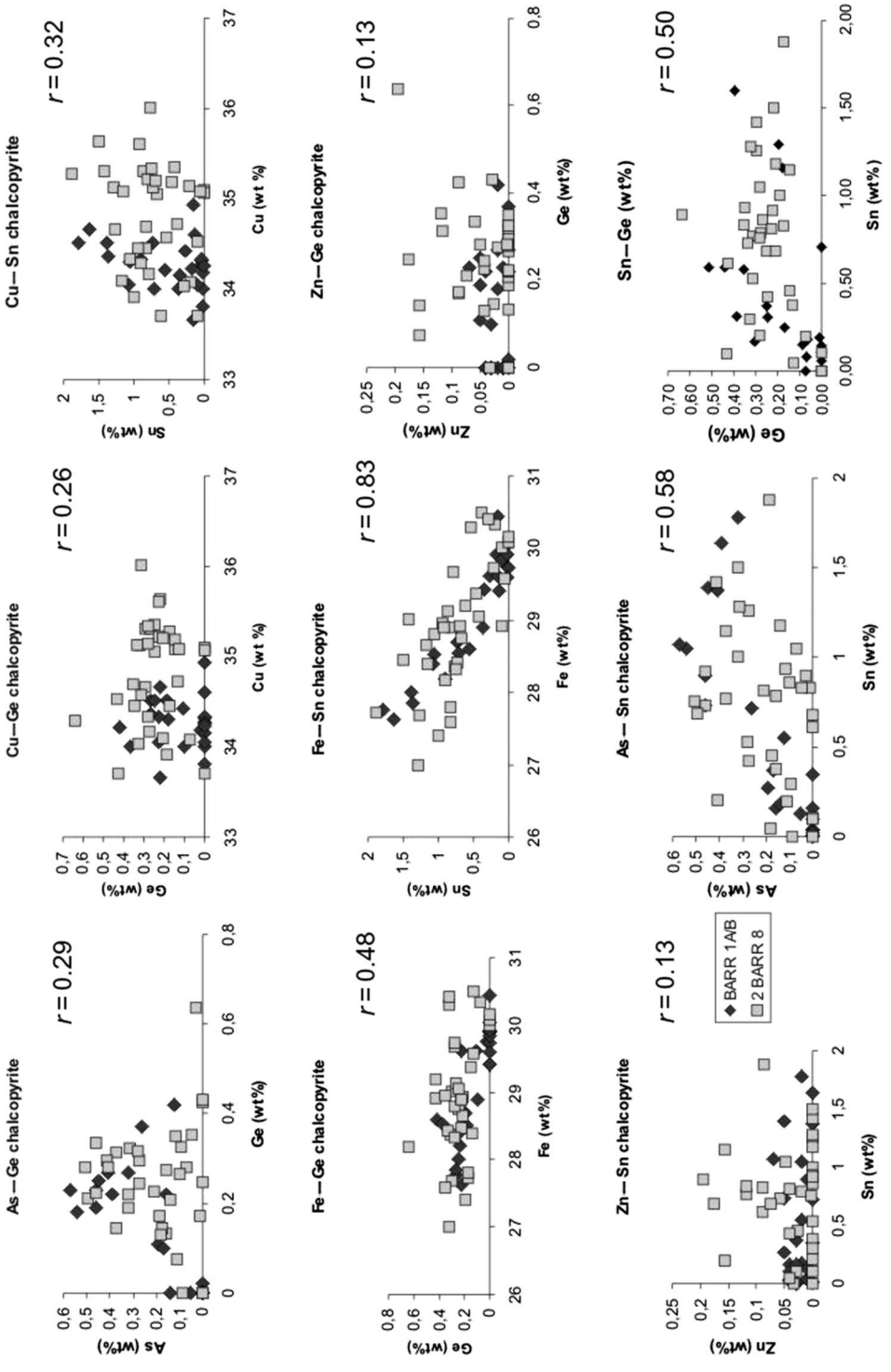

Figure 6. (*Continued*).

Downloaded by [b-on: Biblioteca do conhecimento online ITN] at 07:33 22 March 2012

Table 2. Covariances in the Barrigão whole-rock analysis data-set.

	Cu	Cd	Pb	S	Al	Ca	Bi	Ge	In	Li	Sn	Fe	As	Ag	Sb	Zn
Cu	1	*0,50*	0,47	**0,96**	**–0,77**	–0,28	0,29	*0,64*	0,43	**–0,83**	**0,75**	**0,75**	0,46	0,19	0,46	0,37
Cd		1,00	0,14	0,34	–0,32	–0,35	**0,82**	–0,01	**0,87**	–0,35	–0,07	–0,10	**0,84**	*0,64*	*0,64*	**0,98**
Pb			1,00	*0,50*	–0,25	–0,28	–0,12	0,24	–0,03	–0,22	*0,58*	0,40	0,03	–0,02	0,20	0,06
S				1,00	**–0,74**	–0,34	0,09	**0,70**	0,31	**–0,80**	**0,84**	**0,88**	0,25	–0,02	0,28	0,22
Al					1,00	–0,19	–0,15	–0,39	–0,34	**0,92**	*–0,55*	*–0,68*	–0,20	–0,13	–0,20	–0,26
Ca						1,00	–0,11	–0,21	–0,24	–0,20	–0,25	–0,15	–0,24	–0,09	–0,25	–0,33
Bi							1,00	–0,29	**0,79**	–0,21	–0,34	–0,33	**0,94**	*0,66*	*0,52*	**0,82**
Ge								1,00	–0,15	–0,42	**0,87**	**0,76**	–0,04	–0,17	0,11	–0,15
In									1,00	–0,42	–0,20	–0,10	**0,73**	*0,69*	*0,66*	**0,88**
Li										1,00	*–0,52*	*-0,69*	–0,25	–0,08	–0,28	–0,26
Sn											1,00	**0,92**	–0,11	–0,29	0,01	–0,19
Fe												1	–0,20	–0,41	–0,12	–0,20
As													1,00	**0,71**	*0,66*	**0,80**
Ag														1,00	**0,88**	*0,63*
Sb															1,00	*0,56*
Zn																1,00

Covariances in Barrigão whole-rock analyses. Interpretation has to be done with caution due to the limited number of samples (n = 10).

being marginal, are most likely connected to the tennantite-tetrahedrite phases. Other good correlation matches are positive covariance (>0.8) between Zn–As and Zn–Cd as well as As–Bi and As–Cd, elements contained in the the tennantite-tetrahedrite series. However, interpretation of these data has to be done with caution, due to the small number of samples analysed.

EPMA and Micro-PIXE analysis

Chalcopyrite

Electron backscatter (EBS) images confirm the presence of three different types of chalcopyrite (Figure 9a). Stage (I) chalcopyrite of the 'primary' ore assemblage is relatively inclusion-free, apart from relict pyrite inclusions. Chalcopyrite belonging to the replacement assemblage (cp II) contains more inclusions and occasionally shows a slight compositional zoning, caused by minor Sn contents and mostly tracing crystal faces.

EPMA and micro-PIXE point analysis revealed that high Sn and Ge contents are present in patchy zoned chalcopyrite (cp III) of the hydrothermal overprint assemblage (ore stage III) and in minute sulphide phases, occasionally occurring in zoned chalcopyrite or in small vugs within or near this zoning (Figures 9b, d). In one sample, minute inclusions of potential sphalerite (<1 μm) have been detected in chalcopyrite (II) margins by means of reflected light microscopy. These inclusions are too small to be analysed properly. They probably are preserved relics of almost complete tennatite replacement. The patchy zoning itself is an irregular or schlieren-like zoning, but in places it can be more regular and apparently trace former crystal faces or follow crystallographic directions (Figures 10a, b). In most cases, the patchy zoning is strongly associated with abundant quartz inclusions, which seem to have formed coeval with or slightly post-date the formation of the patchy chalcopyrite zoning. This chalcopyrite zoning is usually accompanied by anhedral tennantite relics. The tennantite relics are strongly affected by an arsenic-rich overprint, pre-dating the euhedral quartz inclusions. Patchy zoned chalcopyrite contains up to 0.64 wt.% Ge and 1.88 wt.% Sn with averages of 0.19 wt.% and 0.55 wt.% for Ge and Sn in 82 EPMA analysis points, respectively (Table 3). The value range for Ge obtained by micro-PIXE analysis is about the same (0.07–0.62 wt.%), which confirms the accuracy of the EPMA data (Table 4). However, we have to note that the obtained micro-PIXE point analysis data can only be considered to be semi-quantitative due to a reduced analysis program with the absence of some elements. The average composition of Sn–Ge-rich chalcopyrite corresponds to a structural formula of $Cu(1.02)Fe(0.96)Sn(0.01)Ge(0.01)S_2$, calculated from 60 EPMA analysis points by normalizing to two sulphur atoms. Hence Sn–Ge-rich chalcopyrite is significantly Fe-deficient with simultaneous enrichment in Cu. The occurrence of Sn in chalcopyrite is coevally associated with the occurrence of As, the latter showing values up to 0.6 wt.%. Sn-free chalcopyrite is also free of As. Zinc does not show any correlation with Sn or Ge.

Regarding all chalcopyrite analysis points, strong negative correlation occurs between Fe and Sn ($r = -0.8$) and some positive correlation between Sn and Ge ($r = 0.5$). The correlation between Fe and Ge ($r = -0.5$) is also negative, whereas Cu–Ge and Cu–Sn do not show any covariance (Figure 6b). Arsenic shows some positive correlation tendency to Sn. Regarding the samples individually, e.g. Barr 1 as a representative of the replacement assemblage (ore stage II) with some overprint texture (ore stage III) and 2 Barr 8 as an example which also suffered additional supergene overprint (ore stage IV), more details come out (Figure 6b). On sample 2 Barr 8, a higher scatter of Zn and Cu compared to Barr 1 can be observed; in particular, the Cu values are generally higher, indicating a late overprint by Cu-rich fluids. Chalcopyrite in sample 2 Barr 8 is slightly more enriched in Ge. The main trace element tendencies are, however, the same in both sample types.

Downloaded by [b-on: Biblioteca do conhecimento online ITN] at 07:33 22 March 2012

Downloaded by [b-on: Biblioteca do conhecimento online ITN] at 07:33 22 March 2012

Table 3. EPMA analysis of Sn–Ge–rich chalcopyrite. All data is listed in wt%.

Sample	Barr 1A	Barr 1A	Barr 1A	Barr 8B	2 Barr 8	2 Barr 8	2 Barr 8	2 Barr 8	2 Barr 8	2 Barr 8	Barr 3-1	Barr 3-1
Hg	–	0,03	0,03	–	–	–	–	–	0,18	–		0,10
S	34,81	34,87	34,46	34,66	34,21	34,44	34,15	34,03	33,79	33,67	34,46	34,36
As	0,32	0,39	0,47	0,34	0,10	0,18	0,37	0,42	0,19	0,03	0,38	0,02
Fe	27,76	27,62	28,22	27,26	29,13	29,37	28,39	29,01	27,73	28,18	28,40	30,48
Cd	0,00	0,01	–	–	0,02	–	0,04	–	–	0,10	0,08	0,11
Se	–	–	–	–	–	–	0,15	–	–	0,03	0,02	
Ag	0,06	–	–	0,01	0,02	0,03	–	0,01	–	0,04		
Ge	0,27	0,22	0,20	0,30	0,27	0,15	0,14	0,30	0,17	0,64	0,41	0,15
Cu	34,52	34,67	35,41	35,31	35,31	35,19	35,08	35,30	35,28	34,29	35,27	33,85
Sn	1,78	1,64	0,71	1,25	0,86	0,46	1,15	1,42	1,88	0,89	0,65	0,14
Bi	0,06	0,03	–	–	0,07	0,09	0,36	0,09	–	0,38	0,16	0,11
Zn	0,02	0,00	0,05	0,01	–	0,03	0,16	–	0,09	0,19		
Pb	–	–	–	–	0,01	0,10	0,05	–	0,05	0,15	0,03	0,09
Co	–	–	0,05	0,03	0,06	0,04	–	–	–	–	0,12	0,04
V	–	–	–	0,01	–	0,01	0,01	0,06	0,03	–	0,00	0,05
Total	99,59	99,49	99,60	99,18	100,06	100,08	100,05	100,63	99,38	98,60	100,00	99,50

Downloaded by [b-on: Biblioteca do conhecimento online ITN] at 07:33 22 March 2012

Table 4. Semi-quantitative micro-PIXE element analyses. All data is listed in wt%.

	2 Barr 16	2 Barr 16	2 Barr 12	2 Barr 8	2 Barr 8	2 Barr 8	2 Barr 8	2 Barr 8
	td	cp	cp	cp	cp	cp	cp	cp
S (Kα)	22,68	30,75	29,90	29,10	28,90	32,04	30,04	29,11
K (Kα)								
Ca (Kα)				0,04	0,02	0,05	0,02	0,02
Fe (Kα)	7,49	32,35	32,21	32,39	30,73	33,25	31,73	31,20
Cu (Kα)	43,23	36,90	37,60	38,47	38,70	32,87	37,41	38,14
Zn (Kα)								
Ge (Kα)			0,07		0,49	0,36	0,62	0,51
As (Kα)	11,12		0,23		0,34	0,78		0,47
Sb (Lα)	15,48							
Sn (Lα)					0,80	0,64	0,18	0,56
Total	100	100	100	100	100	100	100	100

Representative PIXE element analysis for tetrahedrite and chalcopyrite (barren and Si–Ge-rich). Analysis results are semiquantitative and have been obtained by normalizing the analysed elements to 100. The left column lists the analysed elements together with the analytical lines.

Downloaded by [b-on: Biblioteca do conhecimento online ITN] at 07:33 22 March 2012

Tennantite-Tetrahedrite (Fahlore)

Stage (I) tennantite shows typical concentric compositional growth and vector zoning and is generally free of inclusions (Figure 5f). Tennantite of the replacement assemblage (ore stage II) is rich in inclusions of arsenopyrite, chalcopyrite, and löllingite, being the main replacement products. Hydrothermal overprint (ore stage III) led to mineral disequilibrium and patchy zoning, similar to the zoning which has been described as typical of Sn–Ge-rich chalcopyrite. Furthermore, it produced internal micro-veining, micro-brecciation, and re-mobilization, which culminated in the separation of As- and Sb-rich (tetrahedrite) phases. This is primarily recorded in As- or Sb-rich micro-veins cross-cutting earlier tennantite as well as in compositional zoning along tennantite margins (Figure 9c). The most striking textural observation is that of sharply bordered As-rich zones that continue into patchy zoned chalcopyrite, indicating that the same overprint-associated re-mobilization process affected both tennantite and chalcopyrite along distinct zones, interpreted to be associated to fractures (Figures 8 and 9c).

Tennantite and tetrahedrite do not exhibit any Ge content beyond analysis background. They are generally Fe-rich and contain little or no Ag and Zn. When using the Td_x index of $(Sb/(Sb + As)) \times 100$ (Wu and Petersen 1977), most of the fahlore ranges between a Td_x of 20 and 40, therefore being more of tennantite end-member composition. However, Td_x of up to 67 and therefore phases tending more to tetrahedrite end-member composition exist in the hydrothermal overprint paragenesis. Fahlore with composition close to either pure tetrahedrite or tennantite end-member chemistry is located in cross-cutting micro-veins and along re-mobilization zones, therefore clearly being of late-stage origin.

Pyrite and löllingite

Pyrite occurs as relics in stage (I) chalcopyrite or as late supergene phase. Late supergene pyrite is developed as very fine-grained agglomerations associated with or within small veins in chalcopyrite or tennantite. Euhedral löllingite is common as inclusions of a few microns within stage (II and III) chalcopyrite of the replacement and Sn–Ge-bearing hydrothermal overprint assemblage. Like arsenopyrite, it is inferred to be mainly a product of tennantite replacement, which incorporated some of the excess As.

Sn–Ge-bearing copper sulphide

In one sample (Barr 8), EPMA revealed the occurrence of minute sulphide inclusions with sizes of less than a micron within patchy zoned chalcopyrite and in small micro-veins nearby (Figure 9d). Although being too small to facilitate proper analysis, these inclusions roughly show an approximate ratio of 13:1 for Sn and Ge, with approximate values of 4 wt.% and 0.3 wt.%, respectively. Copper is relatively high in these inclusions. The analysed points give Cu (36 wt.%), Fe (24 wt.%), and S (33 wt.%), possibly hinting at a phase related to the stannite group. However, we have to note that in fact only 1/10 of the analysed spots represents the Sn–Ge-bearing copper sulphide, whereas the remaining 9/10 of the analysed volume are contributed from surrounding chalcopyrite.

Element mapping

Element mapping has been used as an effective tool for detection of element distribution, particularly to reveal the distribution of Sn and Ge. EPMA element maps have been

accomplished in areas of patchy zoning previously checked for Sn–Ge content. The strategy for micro-PIXE mapping was slightly different. Element maps have been carried out on promising areas determined through optical microscopy or previous EPMA analysis followed by selective point analysis in sub-zones with high Ge concentration.

Micro-PIXE element distribution mapping confirms Ge to be predominantly contained in chalcopyrite, with zones of strong Ge enrichment corresponding to the patchy disequilibrium zoning observed in EBS images, often directly adjoining unzoned chalcopyrite with little or no traces of Ge (Figure 7). Tennantite does not show significant Ge enrichment above background level. High-resolution analysis of a chalcopyrite area inside a

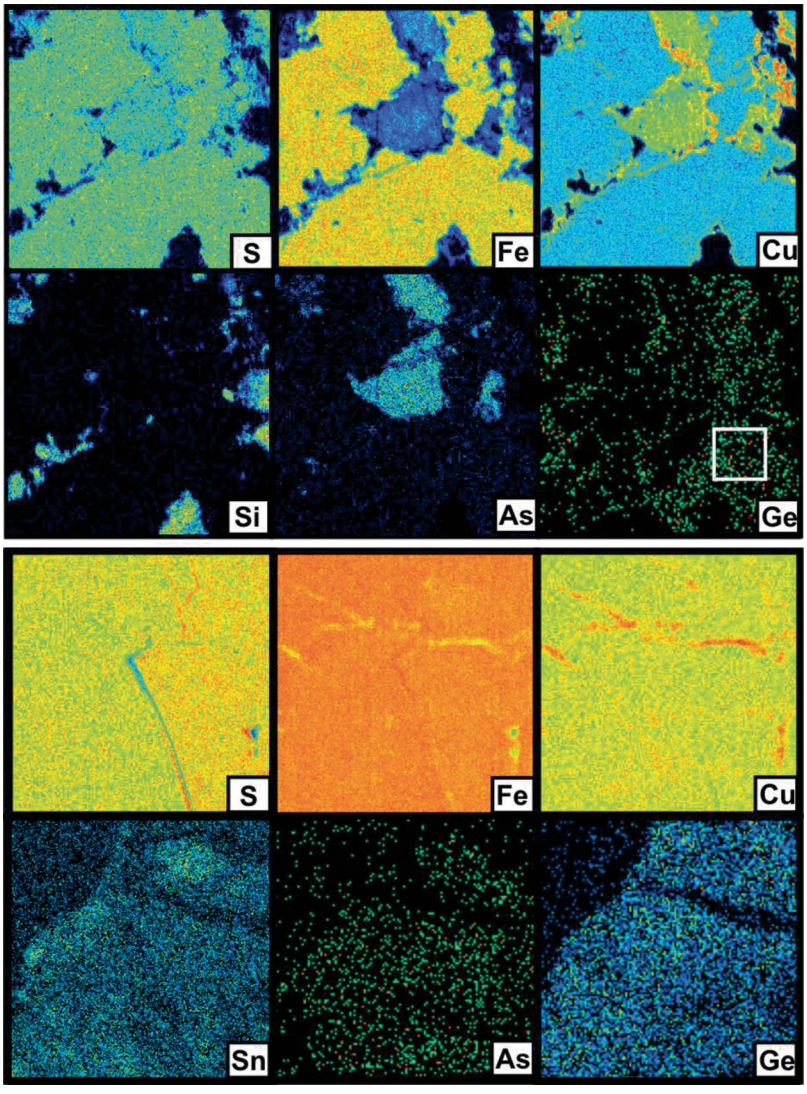

Figure 7. Micro-PIXE element distribution maps of the Sn–Ge-bearing hydrothermal overprint assemblage (2 Barr 8) with supergene copper enrichment along small veins and grain margins. Square side lengths for image (a) are 1320 × 1320 µm. Image (b) is a close-up marked by the white square in image (a) with square side lengths of 264 × 264 µm.

Downloaded by [b-on: Biblioteca do conhecimento online ITN] at 07:33 22 March 2012

high-Ge zone shows a nearly homogeneous distribution of Ge, whereas Sn distribution is slightly more irregular (Figure 7b). From the micro-PIXE element maps it can be concluded that Ge is correlated to Sn and Sn to As, indicating their close association during hydrothermal overprint.

EPMA element maps emphasize and confirm the correlations of Ge with Sn and As observed by micro-PIXE analysis. Distribution of Ge in chalcopyrite is inhomogeneous with high concentration zones next to zones with little or no Ge. Element maps clearly demonstrate Ge and high Sn contents to be restricted to distinct zones in chalcopyrite interpreted to be replacement chalcopyrite affected by element re-mobilization, which took place during hydrothermal overprint. These Sn- and Ge-bearing zones show the patchy disequilibrium compositional zoning referred to earlier, which often involves abundant quartz inclusions. The patchy zoning is most probably the result of mineral disequilibrium, which formed by short-distance selective replacement with migration of elements, possibly through fluid-induced diffusion processes. EPMA element maps propose that hydrothermal re-mobilization affected tennantite and chalcopyrite at the same time along distinct vein-like zones, possibly facilitated by fracture opening. Such re-mobilization-induced zoning often ends abruptly along sharp borders which continue through both phases: chalcopyrite and tennantite-tetrahedrite (Figure 8a). High-resolution element maps show that Ge is clearly associated to Sn but micro-zones with high Sn contents contain lower Ge. This means that, in contrast to element behaviour in whole-rock analysis, and although their behaviour is ambiguous regarding point analysis, in element distribution maps Ge and Sn tend to show negative correlation on the micro-scale (Figures 8c, f and 10c).

Discussion

The mineralogical and geochemical study of the Barrigão copper ore presented in this work provides detailed information about the metal content of this late Variscan mineralized vein structure. The anomalous trace element contents of Sn and Ge in chalcopyrite of this copper ore are most likely the result of a late re-mobilization process which locally affected chalcopyrite and tennantite-tetrahedrite along 'vein-like' zones of different sizes (micron to millimetre width). These zones show a distinct disequilibrium element zoning and are associated to abundant quartz inclusions. Some of the vein-like zones are accompanied by fractures (Figure 9a–c), which could have acted as micro-pathways for Sn- and Ge-bearing fluids. Traces of a Cu-rich Sn–Ge-bearing sulphide phase along or near these vein-like zones support this idea and include the possibility of these trace phases being remnants of a former Sn–Ge-bearing sulphide phase (Figure 9d). The formation of the patchy element zoning, which can be observed along re-mobilization zones, can be explained by sub-microscopic inclusions of Sn–Ge-bearing sulphide phases. Sub-microscopic inclusions of sulphides in other sulphides are known to occur frequently (Pacevski *et al.* 2008). Backscatter electron imaging and element mapping of Barrigão chalcopyrite revealed that the Sn–Ge-bearing patchy zoning is often cloudy or 'schlieren-like' (Figure 9a), but in places also shows a more regular pattern, which seems to trace or copy crystal faces (Figure 10a). Assuming sub-microscopic inclusions to be the reason, there still remains the question of how the inclusions can arrange to display such a zoning, particularly with regard to the occurrence of homogeneous element distribution within a single micro-zone. Where this zoning is well developed down to the micro-scale, opposing behaviours of Sn and Ge can be observed (Figure 10c).

The chemical similarity of Sn and Ge enables substitution of Ge for Sn into the crystal lattice of some Sn-bearing sulphides, e.g. in the stannite group (Bernstein 1985; Höll *et al.*

Downloaded by [b-on: Biblioteca do conhecimento online ITN] at 07:33 22 March 2012

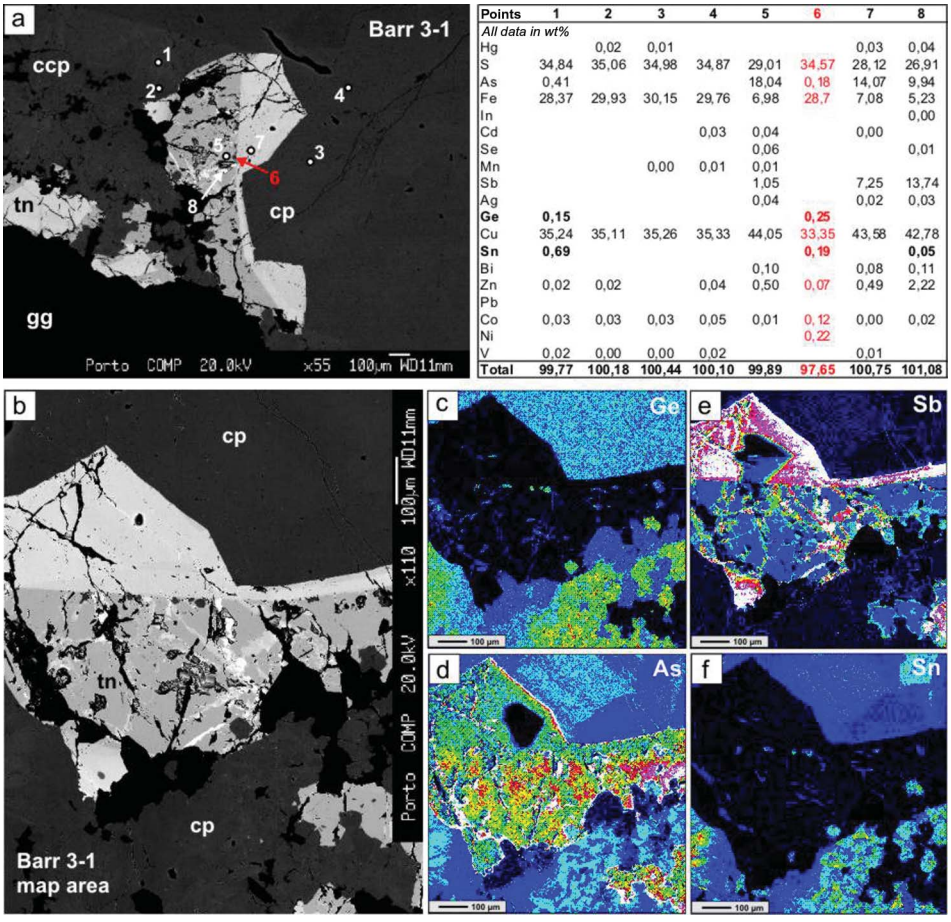

Points	1	2	3	4	5	6	7	8
All data in wt%								
Hg		0,02	0,01				0,03	0,04
S	34,84	35,06	34,98	34,87	29,01	34,57	28,12	26,91
As	0,41				18,04	0,18	14,07	9,94
Fe	28,37	29,93	30,15	29,76	6,98	28,7	7,08	5,23
In								0,00
Cd				0,03	0,04		0,00	
Se					0,06			0,01
Mn			0,00	0,01	0,01			
Sb					1,05		7,25	13,74
Ag					0,04		0,02	0,03
Ge	**0,15**					**0,25**		
Cu	35,24	35,11	35,26	35,33	44,05	33,35	43,58	42,78
Sn	**0,69**					**0,19**		**0,05**
Bi					0,10		0,08	0,11
Zn	0,02	0,02		0,04	0,50	0,07	0,49	2,22
Pb								
Co	0,03	0,03	0,03	0,05	0,01	0,12	0,00	0,02
Ni						0,22		
V	0,02	0,00	0,00	0,02			0,01	
Total	**99,77**	**100,18**	**100,44**	**100,10**	**99,89**	**97,65**	**100,75**	**101,08**

Figure 8. EPMA element distribution map of an area affected by hydrothermal overprint element re-mobilization. (a) Image showing point analysis locations in a tn with adjacent zones of clear unzoned cp and re-mobilized stage (III) replacement cp showing patchy zoning and containing Sn and Ge. Analysis data (in wt.%) is presented in the table. (b) Mapping area (extracted from (a)). (c) Ge distribution map showing the patchy enrichment restricted to the lower zone. (d) Enrichment of As in cp of the lower half of the map accompanies Sn enrichment and developed a more distinct micro-zoning than Ge. The As re-mobilization overprint also affected tn which exhibits a similar zoning pattern. Note the sharp transition border traversing the tn grain. Small grains of Sn- and Ge-rich cp align along this border. (e) Compared to As, the distribution of Sb is precisely of opposing behaviour. (f) Element distribution of Sn in cp correlates with As and Ge. Correlation is particularly strong with As, showing the same micro-zoning in cp.

2007). Generally, the most possible incorporation mechanisms for Ge and Sn in mineral and sulphide phases include diadoch replacement and coupled substitution, with the latter mechanism being responsible for the formation of a range of solid-solution series (Bernstein 1985). Coupled substitution of $Sn^{4+}Fe^{2+}$ for $Fe^{3+}Fe^{3+}$, leading to solid solution towards stannite, has been suggested as an incorporation mechanism for Sn into chalcopyrite in recent black smoker chimneys (Gena *et al.* 2005). Apparently, the strong negative correlation observable between Sn and Fe in Barrigão chalcopyrite (Figure 6b) could hint at such a process. It is highly questionable if coupled substitution could also occur for Ge in

Downloaded by [b-on: Biblioteca do conhecimento online ITN] at 07:33 22 March 2012

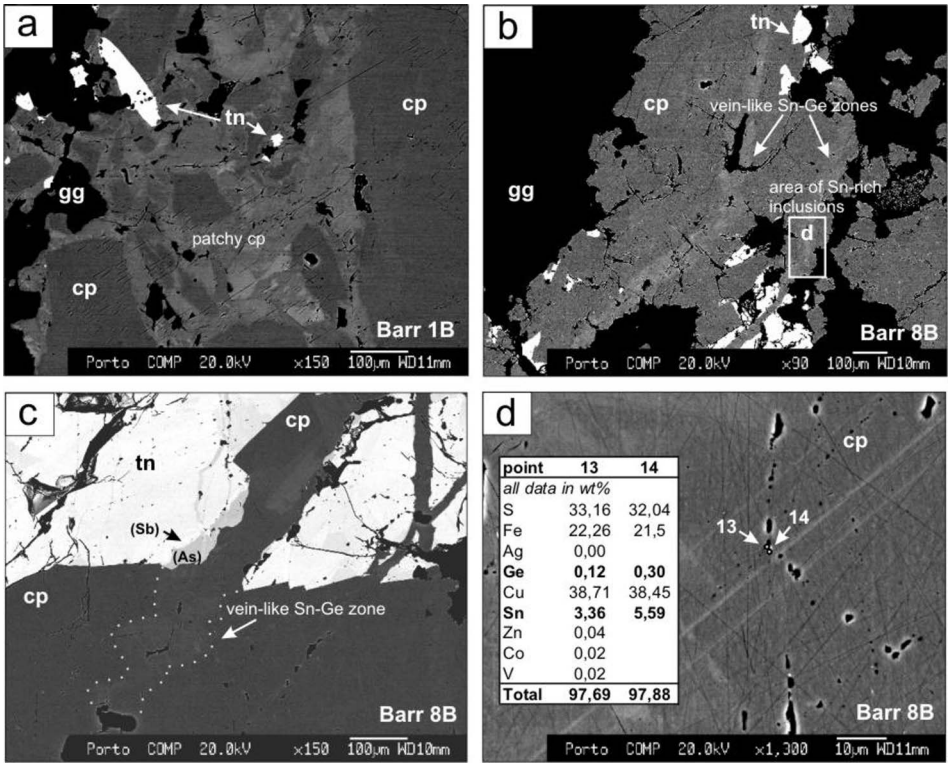

point	13	14
all data in wt%		
S	33,16	32,04
Fe	22,26	21,5
Ag	0,00	
Ge	**0,12**	**0,30**
Cu	38,71	38,45
Sn	**3,36**	**5,59**
Zn	0,04	
Co	0,02	
V	0,02	
Total	**97,69**	**97,88**

Figure 9. EBS images of Sn–Ge-rich patchy zoned cp of the hydrothermal overprint assemblage. (a) Typical replacement texture of Sn–Ge-rich stage (III) cp replacing older stage (II) cp with no or weakly developed zoning. Note the abundant fractures and quartz inclusions and the stage (II) cp relics within the patchy zoned cp. Relics of tn are very common in zoned Sn–Ge-rich cp. (b) Vein-like zones of Sn–Ge-rich cp, associated to vugs and quartz inclusions within weakly zoned cp. Note the lower vein being associated to a fracture in tn. It bears minute inclusions of an unknown but possibly stannite-related Sn- and Ge-bearing sulphide phase. The rectangle marks the location of the close-up (image d). (c) Close-up of a Sn–Ge-rich vein-like zone which seems to have affected tn and cp coevally. The vein-like zone hosts centred vugs and fractures. The chemical process which formed the zoned Sn–Ge enrichment in cp is also responsible for the re-mobilization and chemical overprint reactions in tn along the overprint zones. (d) Location and semi-quantitative analysis of an inclusion of the unknown Sn- and Ge-bearing sulphide phase. Analysis data hints at a sulphide which bears more Cu and Sn, some Ge, and less S and Fe (compared to cp).

the case of chalcopyrite. In Barrigão chalcopyrite point analyses, Ge shows a negative correlation tendency in relation to Fe and some positive correlation to Sn. This means that usually an Fe deficiency accompanies Sn and Ge in chalcopyrite. Germanium only occurs in chalcopyrite, which also contains significant Sn. High-resolution element maps, however, reveal the tendency to an opposing behaviour of both elements on the micro-scale. Micro-zones which show a very high Sn intensity are low in Ge and vice versa (Figure 10c).

Germanium entering for Fe in chalcopyrite through coupled substitution could be imaginable by regarding the formula and crystal structure of briartite $Cu_2(Fe,Zn)GeS_4$, which is similar to that of chalcopyrite and stannite. It is the germanium-equivalent of the stannite-kesterite solid-solution series, and the stannite group minerals are known to be able to incorporate significant amounts of Ge (Bernstein 1985). Briartite and other Ge-bearing sulphides have also been reported to occur as microscopic inclusions in

Downloaded by [b-on: Biblioteca do conhecimento online ITN] at 07:33 22 March 2012

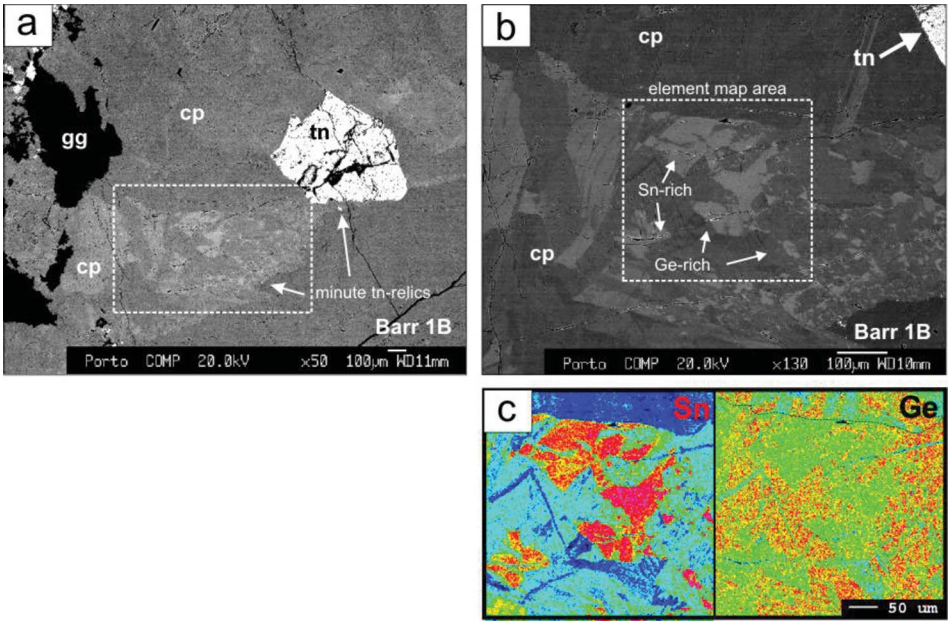

Figure 10. EBS images and EPMA element maps of Sn–Ge-rich cp. (a) Typical patchy zoned cp within weakly zoned (upper part) and unzoned cp (lower part). Note the minute tn relics along the lower zone border. The rectangle marks the location of the close-up (image b). (b) Close-up of the Sn–Ge-zoning showing internal textures like fracturing and replacement. Sn-rich zones are brightest and Ge is most enriched in the zones with an intermediate shade of grey. The rectangle corresponds to the location of the element map (image c). (c) Internal element distribution of Sn and Ge in the patchy zoned cp.

tennantite and chalcopyrite (Melcher *et al.* 2006; Kamona and Friedrich 2007). Briartite is relatively Zn-rich (usually 6–12 wt.%). EPMA and micro-PIXE analyses of Ge-bearing chalcopyrite from the Barrigão ore rarely show Zn contents above the detection limit (Tables 3 and 4). For sphalerite, it has been proved that Ge can substitute for Zn (Höll *et al.* 2007). However, the lack of significant Zn in the Ge-rich chalcopyrite clearly obviates the involvement of briartite or sphalerite as sub-microscopic inclusions or as a component of any hypothetic solid solution. The crystal structure of chalcopyrite, which is a sphalerite derivate, theoretically suggests that Ge could potentially enter for Fe through coupled substitution towards a stannite group phase. Although there is no clear evidence for such an assumption yet, it also cannot be totally ruled out. The possibility of Ge substituting for Fe in chalcopyrite and resulting in lattice expansion along the *c*-axis has been proposed by Takeno (1975).

The observed replacement textures on Barrigão chalcopyrite, which are often associated to tennantite relics (Figures 5a and 9a), suggest the possibility that Ge and Sn, previously contained in tennantite or in inclusions of other Sn- and Ge-bearing phases therein, have been somehow incorporated into the second-stage chalcopyrite (cp II). Late hydrothermal re-mobilization led to further replacement and zonal, vein-like enrichment of Sn and Ge in chalcopyrite of ore stage III, either as sub-microscopic inclusions or as solid solution towards a stanniferous (possibly stannite-related) sulphide phase.

A second question to be discussed is that of the sources for Sn and Ge. Regarding the proximity of the Neves Corvo deposit together with the fact that the formation of the Barrigão copper veins is clearly fault-related, a strong genetic association to Neves Corvo

Downloaded by [b-on: Biblioteca do conhecimento online ITN] at 07:33 22 March 2012

ore re-mobilizations (Moura 2008) is very likely. Some ores of the Neves Corvo deposit have been mined for Sn (cassiterite ore of the 'tin corridor') and other ore types are described to contain Ge values of 10–60 ppm (Höll *et al.* 2007). Considering the high Sn contents in the Neves Corvo deposit, fault-related tectono-metamorphic re-mobilization from Neves Corvo ores could be the source for Cu, Sn, and Ge in the Barrigão copper ore. The similar Cu enrichment of the Barrigão ore and the Neves Corvo copper-rich massive sulphide and tin-bearing cupriferous massive sulphide ores (MC type and MS type, respectively), together with the proximity of both deposits, with a distance of approximately 10 km between Barrigão and the Cu- and Sn-rich Graça ore body, suggests some kind of relation between these two deposits in terms of ore metallogenesis (Figure 6a). In the case of Neves Corvo, late fluid-assisted Cu-rich re-mobilization processes lead to zones of strong Cu enrichment, mainly associated to fault activity (Relvas *et al.* 2006). The high Sn contents in some ore types of the Neves Corvo deposit characteristically differ from other massive sulphide deposits in the IPB and involve additional, possibly magmatic metal sources provided by a near sub-volcanic intrusion (Pinto *et al.* 1997; Relvas *et al.* 2006).

Further regional studies on mineralized vein structures in the South Portuguese Zone have to be conducted in view of the fact that some of these structures are located near massive sulphide ore bodies, e.g. the Barrigão, Brancanes, and Porteirinhos copper veins, which are located close to the Neves Corvo deposit. Other mineralized vein structures are located in barren host units (flysch turbidites of the Mértola Formation) without direct correlation to massive sulphide deposits, e.g. the Ferrarias (Cova dos Mouros) and Martinlongo copper veins. A proper analysis of the metal content of such vein ores could likely provide useful data for further massive sulphide exploration within the IPB.

Acknowledgements

The main author would like to thank Professor Dr Jochen Schlüter (University of Hamburg) for the acquisition of a germanite sample. This work was financially supported by the Portuguese Foundation for Science and Technology (FCT-MCTES) through project PTDC/CTE-GIN/67027/2006 (INCA Project).

References

Benzaazoua, M., Marion, P., Pinto, A., Migeond, H., and Wagner, F.E., 2003, Sn and indium mineralogy within selected samples from the Neves Corvo ore deposit (Portugal): A multidisciplinary study: Minerals Engineering, v. 16, p. 1291–1302.

Bernstein, L.R., 1985, Germanium geochemistry and mineralogy: Geochimica et Cosmochimica Acta, v. 49, no. 11, p. 2409–2422.

Carvalho, D., 1982, New paths to massive sulphide exploration in the Iberian Pyrite Belt: Comunicações Serviços Geológicos de Portugal, v. 68, no. 2, p. 149–162.

Cassard, D., Chabod, J.C., Marcoux, E., Bourgine, B., Castaign, C., Gros, Y., Kosakevich, A., Moisy, M., and Viallefond, L., 1996, Mise en place et origine des minéralisations du gisement à Zn, Ge, Ag, (Pb, Cd) de Noailhac-Saint-Salvy (Tarn, France): Chronique de la Recherche Miniére, v. 514, p. 3–37.

Cook, N., Ciobanu, C.L., Pring, A., Skinner, W., Shimizu, M., Danyushevsky, L., Saini-Eidukat, B., and Melcher, F., 2009. Trace and minor elements in sphalerite: An LA-ICPMS study: Geochimica et Cosmochimica Acta, v. 73, no. 16, p. 4761–4791.

De Oliveira, D.P.S., Matos, J.X., Rosa, C.J.P., Rosa, D.R.N., Figueiredo, M.O., Da Silva, T.P., Guimarães, F., Carvalho, J.R.S., Pinto, Á.M.M., Relvas, J.R.M.S., and Reiser, F.K.M., The Lagoa Salgada orebody, Iberian Pyrite Belt, Portugal: Geology, Distribution, Mineralogy and Geochemistry of Indium. (submitted)

Ferreira, J.A., Figueiredo, M.O., and Gaspar, O., 1995, Estudo cristaloquímico preliminar das tetraedrites do jazigo de cobre filoniano do Barrigão (Faixa Piritosa Portuguesa): Portugal, Memória nº 4, Museu e Laboratório Mineralógico e Geológico, Universidade do Porto, p. 625–627.

Downloaded by [b-on: Biblioteca do conhecimento online ITN] at 07:33 22 March 2012

Gang, D., Xinguo, Z., Querol, X., Izquierdo, M., Alastuey, A., Moreno, T., and Font, O. 2009, Ge distribution in the Wulantuga high-Ge coal deposit in the Shengli coalfield, Inner Mongolia, northeastern China: International Journal of Coal Geology, v. 78, no. 1, p.16–26.

Gaspar, O.C., 1996, Microscopia e petrologia de minérios aplicadas à génese, exploração e mineralurgia dos sulfuretos maciços dos jazigos de Aljustrel e Neves-Corvo: Estudos Notas e Trabalhos do Instituto Geológico e Mineiro, v. 38, p. 3–195.

Gena, K., Chiba, H., and Kase, K. 2005, Sn-bearing chalcopyrite and plainum-bearing bismuthinite in the active Tiger Chimney, Yonaguni Knoll IV seafloor hydrothermal system, South Okinawa Trough, Japan: Okayama University Earth Science Reports, v. 12, no. 1, p. 1–5.

Grime, G.W., 1996, The 'Q factor' method: Quantitative microPIXE analysis using RBS normalisation: Nuclear Instruments and Methods in Physics Research, v. B109, p. 170–174.

Grime, G.W., and Dawson, M., 1995, Recent developments in data-acquisition and processing on the Oxford scanning proton microprobe: Nuclear Instruments and Methods in Physics Research, v. B104, p. 107.

Guberman, D.E., 2009, Germanium [online]. USGS Mineral Commodity Summaries, January 2009, 66–67. Available from: http://minerals.usgs.gov/minerals/pubs/mcs/ [Accessed 30 November 2009].

Höll, R., Kling, M., and Schroll, E., 2007, Metallogenesis of germanium – A review: Ore Geology Reviews, v. 30, p. 145–180.

Johan, Z., 1988, Indium and germanium in the structure of sphalerite: an example of coupled substitution with copper: Mineralogy and Petrology, v. 39, p. 211–229.

Kamona, A.F., and Friedrich, G.H., 2007, Geology, mineralogy and stable isotope geochemistry of the Kabwe carbonate-hosted Pb–Zn deposit, central Zambia: Ore Geology Reviews, v. 30, p. 217–243.

Leistel, J.M., Marcoux, E., Thiéblemont, D., Quesada, C., Sánchez, A., Almodóvar, G.R., Pascual, E., and Sáez, R., 1998, The volcanic-hosted massive sulphide deposits of the Iberian Pyrite Belt. Review and preface to the special issue: Mineralium Deposita, v. 33, p. 2–33.

Mateus, A., Matos, J., Rosa, C., and Oliveira, V., 2003, Cu-ores in quartz-carbonate veins at Estremoz-Alandroal and Barrancos-Sto Aleixo regions (Ossa Morena Zone): A result of Late-Variscan hydrothermal activity?: Ciências da Terra, V (UNL), Lisboa, F90–F93.

Matos, J.X., and Rosa, C., 2001, Diagnóstico Preliminar de Minas Abandonadas. Área Sul. Internal Report, IGM.

Matos, J.X., Martins, L., and Rosa, C., 2003, Parque Mineiro da Cova dos Mouros: IGM contribute for the sustainable development of the mining park: Instituto Geológico y Minero de España, Cuadernos del Museo Geominero, v. 2, p. 487–494.

Maxwell, J.A., Campbell, J.L., and Teesdale, W.J., 1995, The Guelph-PIXE software package-II: Nuclear Instruments and Methods in Physics Research, v. B95, p. 407.

Melcher, F., Oberthür, T., and Rammlmair, D., 2006, Geochemical and mineralogical distribution of germanium in the Khusib Springs Cu–Zn–Pb–Ag sulphide deposit, Otavi Mountain Land, Namibia: Ore Geology Reviews, v. 28, p. 32–56.

Moura, A., 2008, Metamorphosed and metamorphogenic ores of the Neves Corvo volcanogenic massive sulphide deposit, Iberian Pyrite Belt, Portugal: International Geology Review, v. 50, no. 1, p. 89–96.

Oliveira, J.T., Relvas, J.M.R.S., Pereira, Z., Matos, J.X., Rosa, C.J., Rosa, D., Munhá, J., Jorge, R., and Pinto, A., 2006, O Complexo vulcano-sedimentar da Faixa Piritosa: estratigrafia, viulcanosmo, mineralizações associadas e evolução tectono-estratigráfica no contexto da zona Sul-Portuguesa, *in* Dias, R., Araújo, A., Terrinha, P., and Kulberg, J.C., eds., Geologia de Portugal no contexto da Íberia, VII Cong. Nac. Geologia: Portugal, Universidade de Évora, p. 207–244.

Pacevski, A., Libowitzky, E., Zivcovic, P., Dimitrijevic, R., and Cvetkovic, L., 2008, Copper-bearing pyrite from the Coka Marin Polymetallic Deposit, Serbia: Mineral inclusions or true solid-solution?: Canadian Mineralogist, v. 46, no. 1, p. 249–261.

Pinto, A., Ferreira, A., Bowles, J.F.W., and Gaspar, O.C., 1997, Mineralogical and textural characterisation of the Neves-Corvo ores. Metallogenetic implications. *in* Barriga, F.J.A.S., ed., SEG Neves Corvo field conference 1997, 11–14 May Lisbon, SEG, p. 90.1997:

Quesada, C., 1991, Geological constraints on the Paleozoic tectonic evolution of tectonostratigraphic terranes in the Iberian massif, Tectonophysics, v. 185, p. 225–245.

Relvas, J.M.R.S., Barriga, F.J.A.S., Ferreira, A., Noiva, P.C., Pacheco, N., and Barriga, G., 2006, Hydrothermal alteration and mineralization in the Neves-Corvo volcanic-hosted massive sulfide deposit, Portugal. I. Geology, mineralogy, and geochemistry: Economic Geology, v. 101, p. 753–790.

Downloaded by [b-on: Biblioteca do conhecimento online ITN] at 07:33 22 March 2012

Rosa, D.R.N., Finch, A.A., Andersen, T., and Inverno, C.M.C., 2009, U–Pb geochronology and Hf isotope ratios of magmatic zircons from the Iberian Pyrite Belt: Mineralogy and Petrology, v. 95, p. 47–69.

Takeno, S., 1975, The pseudobinary system briartite-chalcopyrite: Neues Jahrbuch für Mineralogie Monatshefte, no. 7, p. 294–299.

Taylor, S.R., and McLennan, S.M., 1985, The continental crust: Its composition and evolution: Oxford, Blackwell.

Wu, I., and Petersen, U., 1977, Geochemistry of tetrahedrite and mineral zoning at Casapalca, Peru: Economic Geology, v. 72, p. 993–1016.

Downloaded by [b-on: Biblioteca do conhecimento online ITN] at 07:33 22 March 2012